RINOPOLYCRETE - TOWARDS A CEMENT-FREE AND FULLY RECYCLED CONCRETE

PROJECTO FCT

PTDC/ECI-CON/29196/2017

Recycled inorganic polymer concrete - Towards a cement-free and fully recycled concrete

(RInoPolyCrete)

Task 5 - Report 2

Paving blocks based on alkali-activated aluminosilicate industrial wastes: Experimental plan and results

August, 2022

Financiamento FCT/POCI

Governo da República Portuguesa

União Europeia FEDER

FCT Fundação para a Ciência e a Tecnologia

MINISTÉRIO DA CIÊNCIA E DO ENSINO SUPERIOR Portugal

TABLE OF CONTENTS

LIST OF FIGURES

LIST OF TABLES

ACRONYMS

OPC	Ordinary Portland cement
FA	Fly ash
MIBA	Municipal solid waste incinerator bottom ash (Portuguese source)
F-MIBA	MIBA from the Finnish source
EAFS	Electric arc furnace slag
AAM	Alkali-activated materials
NaOH	Sodium hydroxide
SiO_2	Silicon oxide
Na_2O	Sodium oxide
Na_2SiO_3	Sodium silicate

1 Introduction

Current research has focused on the remarkable growth of the urban land cover phenomena due to the existing significant differences in urbanisation [1, 2]. The expansion of cities has fundamentally changed the basic theory of urbanisation, turning the modern urban area into a complex network of paved surfaces [3, 4]. Nearly every day, individuals spend numerous hours on the road network. Given the variety of activities on urban pavements, it cannot indeed be viewed as a simple infrastructure [5, 6]. The growing complexity of urbanisation has resulted in a diversification of the urban pavement system, which is now made up of lanes for cars, special lanes for bikes, parking spaces, walkways, and squares [7]. According to statistics, around 95% of road users want a clear and immediate visual identification of various urban road system routes [8]. Iraq, Syria, and India are cherry-picked countries from a lot more that lack facilities for pedestrians and non-motorised vehicles. In 2020, around 42% of all traffic deaths in Delhi were pedestrians due to the road infrastructure being biased in favour of cars instead of pedestrians [9]. As a result, the Indian government has unleashed a solid advancement to establish safe and sustainable infrastructure, with an emphasis on pedestrian mobility [10]. However, as urban transportation projects progress and the demand for other infrastructures rise, the need for building materials such as ordinary Portland cement (OPC) and crushed aggregates has increased [10, 11]. While providing facilities for pedestrians and non-motorised vehicles is one of the conditions for sustainable communities, the environmental effect must also be considered [10]. A sustainable city in terms of mobility and transportation is only conceivable if the problem is handled comprehensively [10]. Since OPC production is the cause of 5-8% of global CO_2 emissions [12], urgent investigations for alternate construction materials are required [11] and, rather than disposing of amorphous aluminosilicate-rich industrial and municipal wastes in landfills, its usage in the construction industry may be both environmentally beneficial and cost-effective.

The alkaline activation process of waste with a high content of amorphous aluminosilicates generates a polymerisation reaction producing N-A-S-H or C-(N-)A-S-H gels [13, 14], which show mechanical properties similar to or even greater than those of conventional cement hydration products. The selection of these wastes that will be subjected to the alkaline activation process is a key task since the quality of the activation depends on the characteristics of the source

material. Precursors such as fly ash (FA) are widely known for their high availability of amorphous aluminosilicates, which leads to an activated material with excellent mechanical properties and durability, that being the reason for some calling it the cement of the future [15-17].

Municipal solid waste incinerator bottom ash (MIBA) is of interest due to its continuous generation from the kerbside collection of municipal solid waste (MSW) [18, 19]. In the EU alone, 16 million tonnes of it are generated every year [20] contrary to the phasing out of FA from coal power plants, which, after the Paris Agreement, were progressively discontinued, since 195 countries agreed to initiate an energy transition, abandoning fossil fuels, and directing their efforts towards the production of clean energy [21]. The increase in energy production through renewable sources has increased by 33.7% from 2000 to 2018 [22].

With the progressive increase of MIBA generated, research has been carried out recently related to the optimisation of the variables that influence the alkaline activation process of MIBA. Some of these studies emphasise the optimisation of the alkaline activator [23], the influence of amorphous silica available for activation [24], the influence of the curing method [25], or the need for pre-treatment of the material associated with involving the release of hydrogen from the reaction of metallic aluminium in an alkaline medium [26-28]. The latter topic is considered the main shortcoming of this precursor, since it leads to the dimensional instability of mixes before they set due to the expansion prompted by the release of hydrogen gas, causing a high internal porosity that is reflected in the low mechanical performance of the material [29, 30].

Other aluminosilicate waste precursors, with little change in yearly production over time, are required to ensure a consistent flow in the supply chain. As the steel industry transitions from new steelmaking to a recycling process, one contestant is electric arc furnace slag (EAFS). Its aluminosilicate-rich chemistry suggests it might be the next cement-replacing AAM utilised in concrete. About 190-290 million tonnes of steel slag are produced yearly, with EAFS accounting for 15-20% [31]. The formation of EAFS depends on recycling scrap metal and pig iron, which can be limited in some countries [32]. It is mainly applied as an aggregate replacement for road base course layers and asphalt pavements [33, 34].

This study intends to effectively use industrial and municipal waste by chemical activation (i.e. alkali-activation) to substitute OPC in paving blocks. It contains a description of the plan for

the preparation of alkali-activated paving blocks made with FA, MIBA, and EAFS. A comparative analysis was carried out between the performance of blocks using the aforementioned precursors and conventional ones made of OPC. The investigation first comprised a preliminary testing stage, in which several variables were explored to obtain paving blocks with the highest possible compressive strength. Once these variables were defined, the mixes were formulated precisely, produced and moulded as paving blocks within an extensive testing campaign on the hardened state.

2 Materials and methods

2.1 Binders

Five different binders were used for the production of paving blocks. OPC, FA, MIBA, and EAFS which their chemical composition and particle size distribution are shown in Table 1 and Figure 1, were provided by local companies in Portugal. Moreover, F-MIBA was imported from Finland with limited information given on its characterisation.

Table 1. Chemical composition of the studied binders

Materials	OPC (%)	FA (%)	MIBA (%)	EAFS (%)
SiO_2	15.36	56.27	48.92	17.66
Al_2O_3	4.61	25.47	8.85	10.13
Fe_2O_3	2.49	6.90	6.69	28.48
K_2O	2.49	2.74	1.59	0.03
CaO	55.13	2.27	18.33	28.18
MgO	1.81	1.83	4.02	5.66
Na_2O	0.12	1.29	6.55	0.19
P_2O_5	0.03	0.44	2.52	0.42
SO_3	4.10	0.80	1.36	0.33
TiO_2	0.29	1.14	0.48	0.65
V_2O_5	0.02	0.05	-	0.11
Cr_2O_3	0.43	0.48	0.06	2.38
CuO	0.02	-	0.16	0.02
ZnO	0.04	0.02	0.35	0.02
SrO	0.05	0.10	-	-
Zr	-	0.03	-	-
MnO_2	-	-	0.12	5.44
BaO	-	-	-	0.17

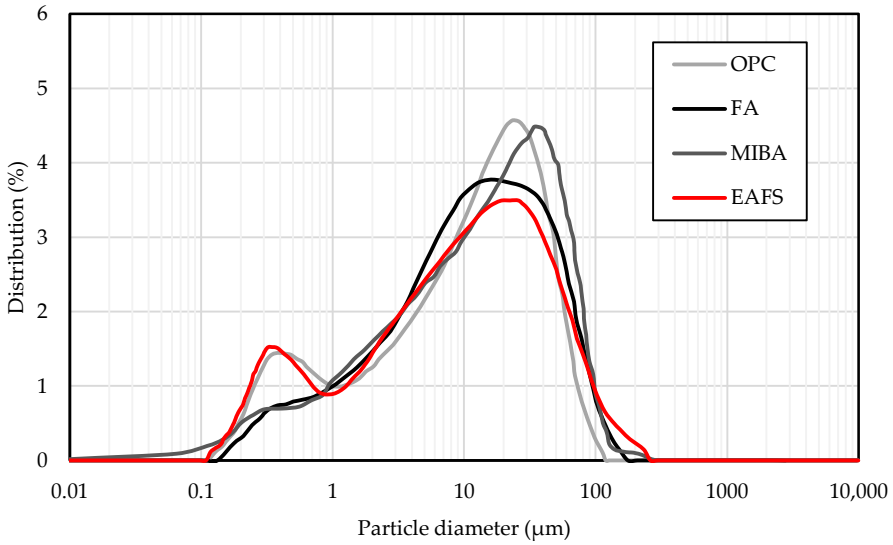

Figure 1. Particle size distribution of the studied binders

2.1.1 Cement

OPC (CEM I 42.5 R) was provided by SECIL-Outão - Portugal, was used as reference binder according to EN 197-1 [35].

2.1.2 Alkali-activated binders

Alkali-activated FA was also considered as a reference binder given the large amount of experience with its use in the literature. Additionally, three other different precursors were alkali activated and used as binders for producing the paving blocks.

2.1.2.1 Fly ash

The FA was sourced from EDP - Gestão da Produção de Energia, S.A. at the Sines Power Plant and considered as the reference alkali-activated binder. This binder shows an apparent density of 2431 kg/m^3 and an average particle size distribution of ~20 µm (Figure 1).

2.1.2.2 Municipal solid waste incinerator bottom ash

Two types of MIBA from two different sources were evaluated. One was sourced from Valorsul facility for waste management in São João da Talha, Portugal. This batch required preparation, mainly grinding to achieve cement-like sized particles before it could be used as precursor. The

second type of MIBA, the Finnish MIBA (FMIBA), was sourced from a waste-to-energy power plant in Finland. The FMIBA was shipped already prepared and ready to use as a binder.

2.1.2.3 Electric arc furnace slag

The electric arc furnace slag (EAFS) is a by-product of steel manufacturing and was collected from the Siderurgia Nacional de Portugal, provided by HARSCO. This material presents an apparent density of 3770 kg/m^3 and a particle size distribution similar to that of OPC (~25 µm).

2.2 Alkaline activator

A commercial solution of sodium silicate was used in the experimental campaign, which contains sodium oxide (Na2O) content between 12.7-13.3% and silicon oxide (SiO_2) content between 26.2-26.8%; water content 59.9-61.1% and relative density of 1.296-1.396 g/ml. Additionally, reactive grade sodium hydroxide pellets were also used, with 98% purity and a density of 2.13 g/ml.

2.3 Aggregates

Two types of siliceous sand were used as fine aggregate; 0/4 coarse sand and 0/1 fine sand. Additionally, a sand-gravel 0 (2-5.6mm) of calcareous nature was used. The bulk density, water absorption, humidity, and size were evaluated (Table 2). Before using these aggregates, they were fully dried at 105 ºC. The mass ratio of the fine aggregate was 34 % and 66% for fine and coarse sand, respectively, while the proportion of the total fine aggregates and sand-gravel was 46% and 54%, respectively.

Table 2. Aggregate characterisation

Aggregates	Nominal size	Oven-dried density	Water absorption	Mass ratio	
	mm	kg/m^3	%	%	
Fine sand	0/1	2668	0.3	34	46
Coarse sand	0/4	2582	0.3	66	
Sand-gravel	2/5.6	2657	1.0	-	54

2.4 Water reducing admixture

The SikaPlast-717, a naphthalene-based superplasticiser was used as water-reducing admixture (WRA). It consisted of synthetic organic water-based dispersants with a density of 1.21 ± 0.03 kg/dm^3 and a pH of 10 ± 1.

2.5 Formulation of the mixes

2.5.1 Preliminary design trials

The optimum mixing water content (water/binder ratio) for the highest density was determined based on the Proctor compaction test, frequently used in soil-mechanics. This test was performed for all the binders (OPC, AA-FA, AA-MIBA and AA-EAFS). For that purpose, a range of water/binder ratios (0.20-0.40) was added to the binders and aggregates and mixed in a mechanical paddle mixer. These mixes were then subjected to the Proctor test, the results nominated the optimum water content based on the maximum dry density of the compacted MIBA. However, the mix design, in particularly the water/binder ratio, was insufficient to achieve a decent mechanical performance for the OPC reference paving block. Therefore, an alternative method was conducted to achieve an optimum dry density for all binders and an optimum mechanical performance. This method included preparing small blocks using mortar moulds ($160 \times 40 \times 40$ mm^3) to investigate the fresh state slump initially set at 105 ± 5 mm and the hardened state mechanical performance by varying the w/b ratio and superplasticiser content.

2.5.2 Mix design

The contents of each of the constituents for the production of the blocks are calculated based on a weight ratio of 1:5 (binder: aggregates). The volumetric ratio of SiO_2/Na_2O was defined as 1.0 and the NaOH/precursor ratio as 10. The water/binder ratio varied from binder to binder based on preliminary trials. Table 3 presents the mix formulation for the production of the paving blocks, considering four binders and 16 blocks per binder.

Table 3. Formulation of the mixes for one paving block per binder

Binder type	**OPC**	**FA**	**MIBA**	**EAFS**
W/B ratio	0.35	0.25	0.3	0.3
Binder (g)	700	700	700	700
Water(g)	272	28.5	63.3	65
Superplasticiser (g) (wt% binder)	10.5 g (1.5%)	-	10.5 g (1.5%)	7.0 g (1.0%)
Borax (g) (4%)	-	28	28	28
Fine sand 0/1 (g)	601	582	582	582
Coarse sand 0/4 (g)	1163	1127	1127	1127
Sand-Gravel 2/5.6 (g)	2071	2007	2007	2007
NaOH (g)	-	62	62	62
Na_2SiO_3 solution (g)	-	265	265	265

2.6 Preparation and testing method of the paving blocks

2.6.1 Production method

After the adjustments and the preliminary trials to optimise the dry density, mechanical performance and compaction, each block was produced individually using a mortar mixer. First, the sand gravel and 2/3 of the liquid were mixed for the first 4 minutes. Then, the fine sands were added to the mix for another 2 minutes. Finally, the binder and the rest of the liquid (1/3) were mixed for 4 minutes to have a ready mixed paving block.

A prismatic mould (200 × 100 × 100 mm^3) with a 20-mm metal lid on top was used to prepare the pavement blocks. The mould was half filled with the mixture and compacted with 20 strokes using a plastic rod. The second layer was added until the mould was full and subjected to additional 20 strokes. Finally, a metal lid (i.e. compactor) was placed on top of the third layer before compacting it using a mechanical compressor at 125 ± 25 kN.

After mechanical compaction, block demoulding was made by extrusion with the help of a wood extruder, making sure that it and the mould were in-line. To that end, the block was firmly pushed through the mould, by applying a force in the wood extruder perpendicular to the surface of the block. The final outcome of this process was a 200 × 100 × 80 mm^3 paving block.

2.6.2 Curing conditions

Once the paving blocks were extruded, they were immediately transported and subjected to thermal curing in an oven for a period of 24 hours at 70 ºC. After this stage, 8 blocks of each family were subjected only to dry curing, and placed in a dry chamber at 20 ± 5 ºC and 60 ± 10% RH, for 28 days (uncarbonated). The other 8 blocks were subjected to dry curing, under the same conditions of the uncarbonated ones, for 21 days, followed by 7 days accelerated carbonation in the carbonation chamber at 5% CO_2, 20 ± 5 ºC and 60 ± 10% RH.

2.6.3 Test methods

Following the curing process, the specimens were subjected to the tests defined in the standard that regulates paving blocks (EN 1338 [36]). These tests were performed for each family of blocks and for each type of curing conditions in accordance with the organogram presented in Figure 2.

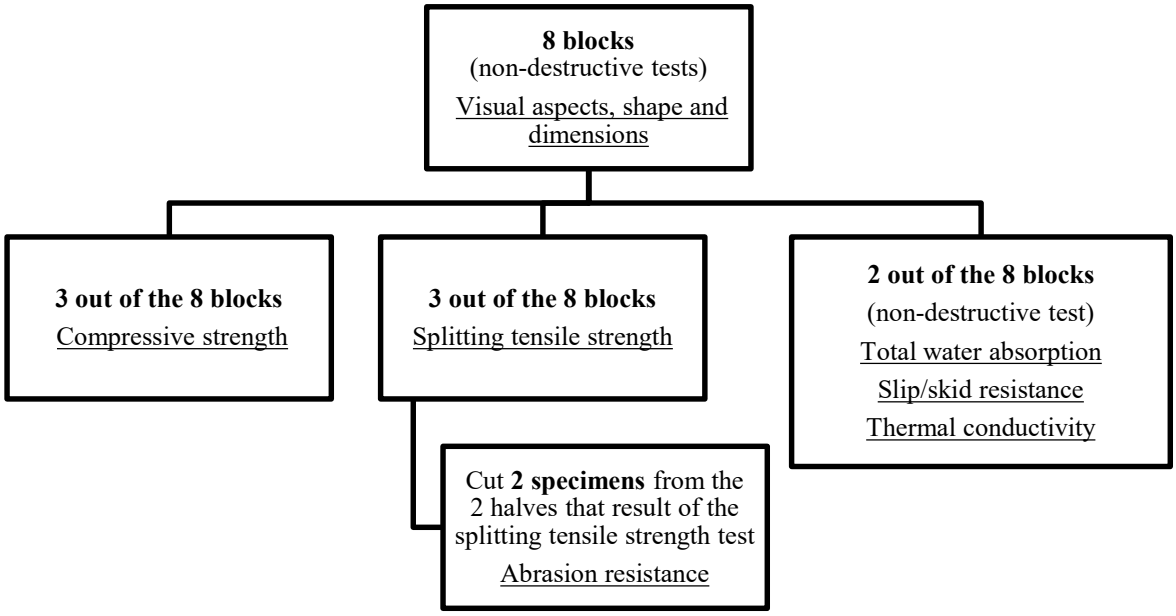

Figure 2. Organogram with the testing sequence for each family of paving blocks and for each of the curing conditions

3 Results and discussion

3.1 Visual aspect, shape and dimensions

The blocks' visual aspect, shape and dimensions were inspected according to standard EN 1338 [36]. This test comprised a careful visual inspection of all blocks to check their homogeneity, uniformity in terms of texture and dimensions, the flatness of their faces and the presence of flaws. All specimens showed an offset/deviation in the sizes valuing a ± 3mm after hardening, mainly due to the manual demoulding process that may have led to some variations in the blocks' sizes. Such variations are likely minimised using an industrialised procedure. Other reasons for these variations could be shrinkage, self-settlement, or expansion in blocks containing MIBA, for example. However, all the specimens fell within the limit of the permissible deviation shown in Table 4, except for the FA sample. The FA specimens presented some self-settlement, which caused a lower thickness and higher length/width than the allowable. Therefore, further adjustments must be made to the mix design of the FA specimens despite their low w/b ratio.

Table 4. Permissible deviations [36].

Block thickness (mm)	Length (mm)	Width (mm)	Thickness (mm)
< 100	± 2	± 2	± 3
≥ 100	± 3	± 3	± 4

Note: The difference between any two measurements of the thickness of a single block shall be ≤ 3 mm.

3.2 Slip/skid resistance

The specimens' slip resistance value (USRV) was made using pendulum friction test equipment to evaluate the frictional properties of the sample on the upper face, following EN 1338 [36]. The mean values of the pendulum test obtained are shown in Figure 3. All blocks presented (low to extremely low) slipping potential for carbonated and uncarbonated specimens. OPC and EAFS blocks responded to carbonation as an approach to enhance the slip/skid resistance, while the carbonated FA and MIBA samples had lower resistance to slip compared to the un-carbonated ones.

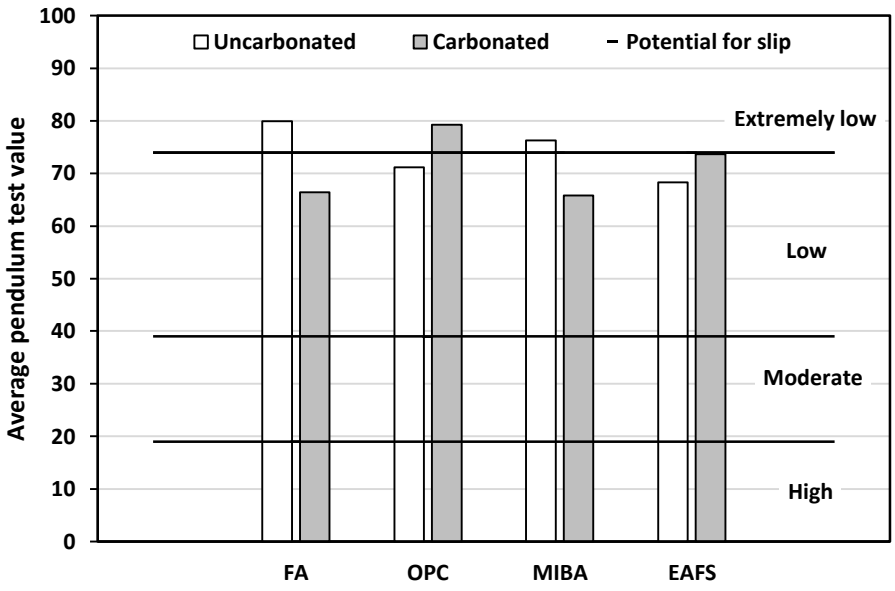

Figure 3. Average pendulum test for paving blocks containing OPC, FA, MIBA, and EAFS.

3.3 Abrasion resistance (Böhme test)

The abrasion resistance of the blocks was determined by the Böhme test in accordance with standard EN 1338 [36]. A square sheet of samples was taken from the blocks and were placed on the Böhme disc abrader, on the test track of which standard abrasive was spread, the disc rotated, and the specimens were subjected to the abrasive load for 16 cycles. The average loss in mass of the carbonated and uncarbonated samples was then recorded, and the abrasive wear as the mean loss in specimen volume ΔV was calculated (**Error! Reference source not found.**), as shown in Figure 4. The FA specimens showed the lowest amount of mass loss due to abrasion (~3.6%), followed by OPC specimens (~7.4%), MIBA (~15.9%) and EAFS (~34%). The latter precursor showed an unexpected considerably larger mass loss and inconsistent with previous results. The uncarbonated specimens (of EAFS) failed when testing them as they broke on the rotating disk during the 16 cycles. Additional research will be carried out to ascertain the reasons behind this worse performance.

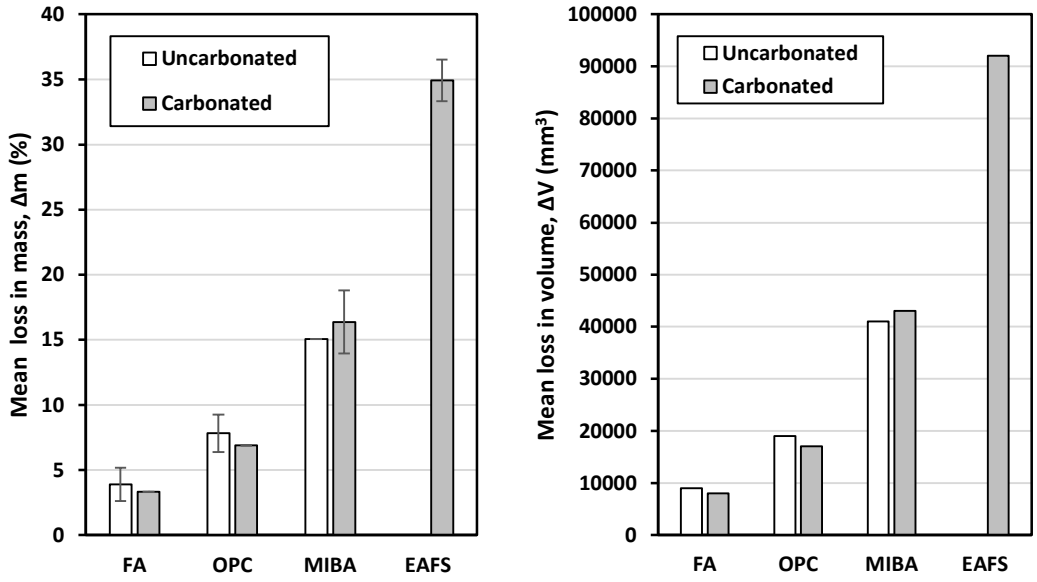

(a) (b)

Figure 4. Abrasion resistance: (a) mean loss in mass after 16 cycles (%); (b) abrasive wear after 16 cycles as the mean loss in specimen volume ΔV

$$\Delta V = \frac{\Delta m}{\rho_R} \quad (1)$$

Where

ΔV	is the loss in volume after 16 cycles in cubic millimetres;
Δm	is the loss in mass after 16 cycles in grams;
ρ_R	is the density of the specimen or, in the case of multi-layer specimens, the density of the wearing layer in grams per cubic millimetre.

3.4 Mechanical performance

The results of the splitting tensile and compressive strength tests are shown in Figure 5. Pavement blocks with alkali-activated FA presented the best performance. Uncarbonated FA specimens had average splitting tensile and compressive strength values of 11.3 MPa and 80.6 MPa, respectively, which are deemed high-grade quality and preferable over OPC blocks, which already performed reasonably well (i.e. 4.12 MPa and 58.6 MPa, respectively). The highly reactive amorphous aluminosilicate phases of FA breakdown in an alkaline medium and subsequently agglomerate as sodium aluminosilicate hydrate (N-A-S-H) polymer chains (mainly in the form of Si-O-Si bridges), resulting in increased strength [37]. Fixing the SiO_2/Na_2O ratio at 1.0 (previously determined in an optimization procedure) resulted in extra Si^{4+} species from the sodium silicate, leading to increased strength. However, although exhibiting a definite binding ability in alkali activation environments, the mechanical performance of MIBA and EAFS was not as good as that of FA blocks. Not only do MIBA and EAFS contain less amorphous phases than FA, resulting in less strength enhancing C-(N)-A-S-H phases, but MIBA also contains a significant quantity of metallic aluminium (e.g. bottle caps, cans, aluminium foil), leading in a severe expansion response. When the aluminium comes into contact with the OH^--rich solution, it oxidizes and emits H_2 gas, resulting in entrained gas pockets and hence increased porosity. Because of this expansion, the produced specimens become somewhat protuberant.

The FA sample showed an unfavourable response to the accelerated carbonation curing process.

This was to be predicted, given other studies have shown comparable results [38, 39]. In the presence of a stable microstructure with extremely low porosity, the addition of CO_2 is likely to disrupt the existing phases, leaving very few pores for $CaCO_3$ precipitation. However, for mixes with low-to-medium mechanical performance (typically associated with mid-high porosity levels), the presence of CO_2 is likely to cause decalcification of Ca-bearing phases (Si-based or otherwise), resulting in the precipitation of carbonates in adjacent empty spaces as well as the formation of amorphous Si gel, which can lead to greater polymer chains [40]. Despite the fact that the authors' earlier experiments demonstrated outstanding outcomes following the carbonation stage [11], the MIBA and EAFS blocks in this investigation exhibited minor variations. This is due to the study's use of bigger and less porous specimens, which take substantially longer time to display the same amount of carbonation under the same circumstances (atmospheric pressure, 5% CO_2 and 60% RH). In fact, after a 7-day carbonation curing, the surface of the broken blocks exhibited a predominantly pinkish hue when a phenolphthalein solution was applied. This suggests that the pH level did not significantly decreased throughout this period (in contrast to what was reported in prior research [11, 29, 30, 41]), implying a moderate carbonation rate.

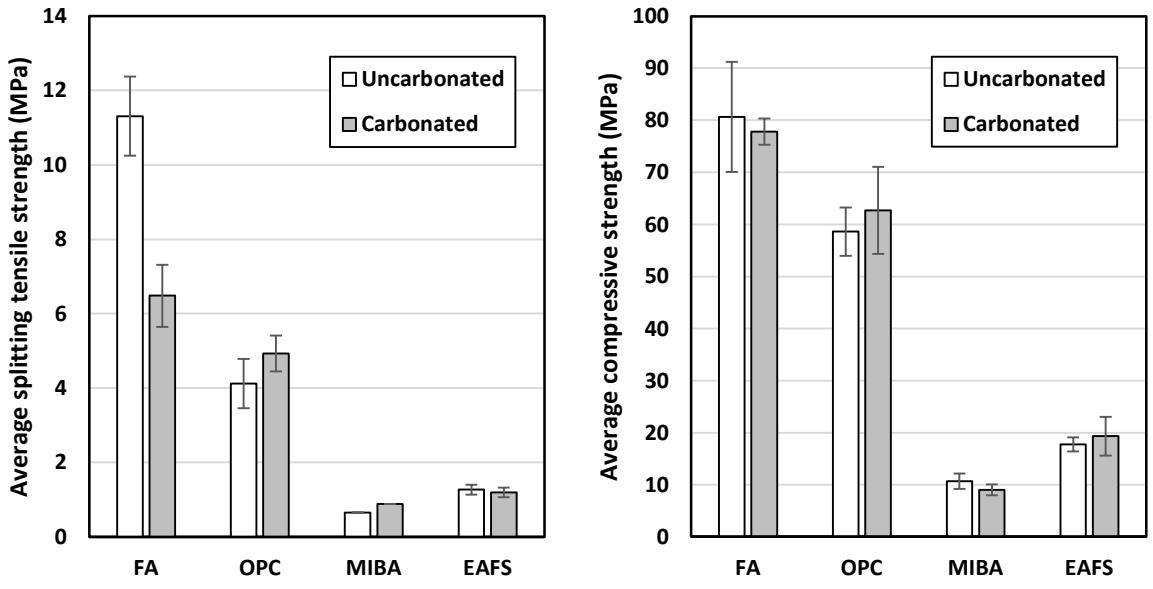

Figure 5. Mechanical performance of uncarbonated and carbonated paving blocks; (a) average splitting tensile strength; (b) average compressive strength.

3.5 Water absorption

The total water absorption was determined according to standard EN 1338 [36] by evaluating the mass loss, in percentage, after a specimen was soaked in water and then oven dried. Figure 6 shows blocks' fully saturated mass (M_1) and fully dry mass (M_2) at oven drying times of 0 to 144 hours, respectively. In addition, the mass loss in percentage was calculated (**Error! Reference source not found.**) for each carbonated and uncarbonated specimen from different binders. The OPC and FA specimens demonstrated a 3.5% to 4.0% water absorption. In contrast, the MIBA and EAFS blocks have absorbed almost twice those of OPC and FA (i.e. ~7% to 10%). Since MIBA and EAFS blocks had more voids and microcracks, it is evident that they can absorb more water. The carbonation stage was expected to have a noticeable effect on reducing the porosity of the specimens. Indeed, slightly lower values were obtained from all blocks. However, it cannot be inferred that it had a real impact on this property. It is likely due to extensive carbonation not being observed in these specimens and thus little overall improvement was observed.

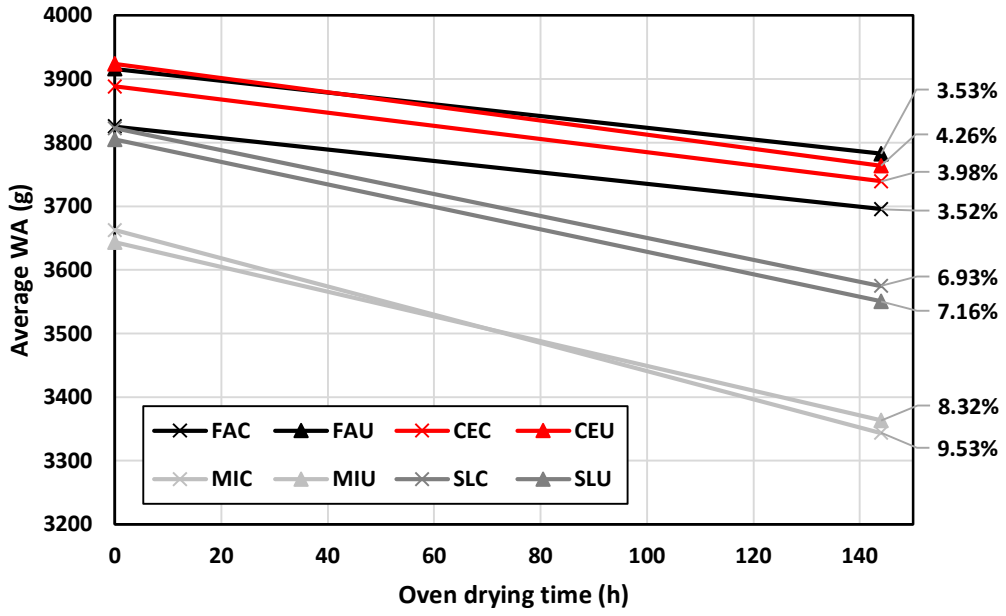

Figure 6. Water absorption by immersion

It is worth mentioning that the standard allocates to a national level in terms of durability requirements for the classes of water absorption. That said, the FA and OPC samples, resulting in less

than 6% water absorption values, fall under (class 1 - mark B). However, the MIBA and EAFS specimens obtained more than the limit stated in the standard. Therefore, additional improvement has to be made in the mix design and the compaction methods to reduce the porosity.

$$W_a = \frac{M_1 - M_2}{M_2} \times 100\ \% \quad (2)$$

3.6 Thermal conductivity

The specimens' thermal conductivity was determined using the ISOMET 2114 device from Applied Precision. Figure 7 presents the results obtained from this test. The FA and OPC specimens clearly showed higher thermal conductivity values than those of MIBA and EAFS specimens. Given the relatively high standard deviation for the former mixes (average values intersecting the range of other mixes), it is not possible to accurately state specific trends. The MIBA and EAFS specimens, however, presented values in line with those seen in previous sections (namely mechanical performance and water absorption). MIBA showed the lowest thermal conductivity values followed by EAFS, thus indicating large porous microstructures thereby diminishing heat transfer. The carbonated specimens presented slightly higher thermal conductivity, which may be indicative of a densification stemming from the precipitation of $CaCO_3$ and the creation of additional Si-O-Si chains with the Si coming from decalcified phases.

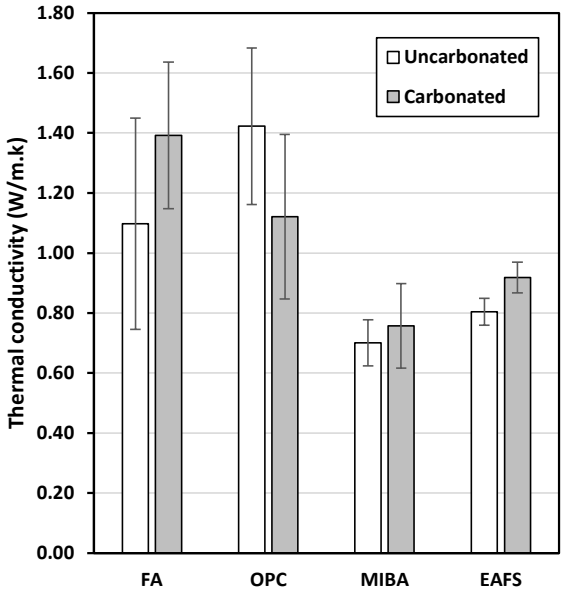

Figure 7. Thermal conductivity

4 Conclusion

The aim of this work was to produce and test pavement blocks made from alkali-activated aluminosilicate industrial waste complying with EN 1338 [36]. This study proved that among all the opposing precursors, FA demonstrated obviously greater reactivity and sufficient composition for alkali activation. When compared to conventional OPC blocks, alkali-activated FA blocks showed higher mechanical performance. However, the carbonation process proved to have a negative impact on the splitting tensile and compressive strengths of FA blocks, but not on OPC specimens, while negligible differences were observed for those containing MIBA and EAFS. Like FA, MIBA and EAFS contain amorphous phases that can react with the alkaline activator thereby leading to a reasonably stable and sturdy construction material though with clearly inferior mechanical performance.

In terms of slip/skid resistance, all the precursors demonstrated comparable results and were suitable for pavement construction. However, the carbonation curing process had no noticeable impact on this property. On the other hand, water absorption and thermal conductivity tests were correlated (inverse proportionality) and indicate a considerably dense microstructure by FA and OPC specimens, whereas MIBA and EAFS blocks presented much higher water absorption and lower thermal conductivity. Then again, the mass loss of FA and OPC specimens

(determined by the abrasion test) were adequate for pavement construction from a durability perspective, unlike those containing MIBA and EAFS.

Overall, MIBA and EAFS still require adjustments before their use as binders in the production of alkali-activated construction materials. In this case, their performance was slightly lower than some of the limits imposed in EN 1338 [36] for the production and conformity of pavement blocks. Nevertheless, these precursors still exhibit an adequate performance to be used in other construction applications, namely masonry blocks, which have less stringent property requirements and for which a lower thermal conductivity is valuable, for example. Additionally, these materials are still in their early stages of research and present a high potential for optimisation and property improvement. In parallel studies using similar formulations, the authors have reached over 30 MPa in compressive strength, thereby opening the possibility of using these materials, otherwise considered as waste, for structural precast elements.

References

1. Artmann, M.; Inostroza, L.; Fan, P., Urban sprawl, compact urban development and green cities. How much do we know, how much do we agree? Elsevier: 2019; Vol. 96, pp 3-9.
2. Seto, K. C.; Güneralp, B.; Hutyra, L. R., Global forecasts of urban expansion to 2030 and direct impacts on biodiversity and carbon pools. *Proceedings of the National Academy of Sciences* **2012,** 109, (40), 16083-16088.
3. Anastasiadou, K.; Vougias, S., "Smart" or "sustainably smart" urban road networks? The most important commercial street in Thessaloniki as a case study. *Transp. Policy* **2019,** 82, 18-25.
4. Ng, C. P.; Law, T. H.; Jakarni, F. M.; Kulanthayan, S., Relative improvements in road mobility as compared to improvements in road accessibility and urban growth: A panel data analysis. *Transportation Research Part A: Policy and Practice* **2018,** 117, 292-301.
5. Gulotta, T.; Mistretta, M.; Praticò, F., A life cycle scenario analysis of different pavement technologies for urban roads. *Science of the total environment* **2019,** 673, 585-593.
6. Tsiotas, D.; Polyzos, S., The topology of urban road networks and its role to urban mobility. *Transportation research procedia* **2017,** 24, 482-490.
7. Lyu, X.; Han, Q.; de Vries, B., Procedural modeling of urban layout: population, land use, and road network. *Transportation research procedia* **2017,** 25, 3333-3342.
8. Harsha, G.; Thoradeniya, B.; Halwatura, R. In *Public perceptions on urban outdoor constructions and their materials*, Proceedings of the 8th International Conference of

Faculty of Architecture Research Unit (FARU), 2015; University of Moratuwa Colombo, Sri Lanka: pp 1-12.

9. The Times of India, News, India news, (2022). https://timesofindia.indiatimes.com/ (July 27, 2022),

10. Hossiney, N.; Sepuri, H. K.; Mohan, M. K.; Arjun, H.; Govindaraju, S.; Chyne, J., Alkali-activated concrete paver blocks made with recycled asphalt pavement (RAP) aggregates. *Case Studies in Construction Materials* **2020,** 12, e00322.

11. Kassim, D.; Lamaa, G.; Silva, R. V.; de Brito, J., Performance Enhancement of Alkali-Activated Electric Arc Furnace Slag Mortars through an Accelerated CO2 Curing Process. *Applied Sciences* **2022,** 12, (3), 1662.

12. Scrivener, K. L.; Kirkpatrick, R. J., Innovation in use and research on cementitious material. *Cem. Concr. Res.* **2008,** 38, (2), 128-136.

13. Khale, D.; Chaudhary, R., Mechanism of geopolymerization and factors influencing its development: a review. *Journal of Materials Science* **2007,** 42, (3), 729-746.

14. Myers, R. J.; Bernal, S. A.; Provis, J. L., A thermodynamic model for C-(N-)A-S-H gel: CNASH_ss. Derivation and validation. *Cem. Concr. Res.* **2014,** 66, 27-47.

15. Bocullo, V.; Vaičiukynienė, D.; Gečys, R.; Daukšys, M., Effect of ordinary Portland cement and water glass on the properties of alkali activated fly ash concrete. *Minerals* **2020,** 10, (1), 40.

16. Fang, G.; Ho, W. K.; Tu, W.; Zhang, M., Workability and mechanical properties of alkali-activated fly ash-slag concrete cured at ambient temperature. *Constr. Build. Mater.* **2018,** 172, 476-487.

17. Farhan, N. A.; Sheikh, M. N.; Hadi, M. N. S., Investigation of engineering properties of normal and high strength fly ash based geopolymer and alkali-activated slag concrete compared to ordinary Portland cement concrete. *Constr. Build. Mater.* **2019,** 196, 26-42.

18. Xuan, D.; Tang, P.; Poon, C. S., Limitations and quality upgrading techniques for utilization of MSW incineration bottom ash in engineering applications–A review. *Constr. Build. Mater.* **2018,** 190, 1091-1102.

19. Blasenbauer, D.; Huber, F.; Lederer, J.; Quina, M. J.; Blanc-Biscarat, D.; Bogush, A.; Bontempi, E.; Blondeau, J.; Chimenos, J. M.; Dahlbo, H., Legal situation and current practice of waste incineration bottom ash utilisation in Europe. *Waste Manage.* **2020,** 102, 868-883.

20. Joseph, A.; Snellings, R.; Nielsen, P.; Matthys, S.; De Belie, N., Pre-treatment and utilisation of municipal solid waste incineration bottom ashes towards a circular economy. *Constr. Build. Mater.* **2020,** 260, 120485.

21. Rogelj, J.; Den Elzen, M.; Höhne, N.; Fransen, T.; Fekete, H.; Winkler, H.; Schaeffer, R.; Sha, F.; Riahi, K.; Meinshausen, M., Paris Agreement climate proposals need a boost to keep warming well below 2 C. *Natur* **2016,** 534, (7609), 631-639.

22. EP *Cohesion policy and climate change - Annex A : Regional development*; QA-05-21-043-EN-N; European Parliament (EP): 2021; p 111.

23. Huang, G.; Yang, K.; Sun, Y.; Lu, Z.; Zhang, X.; Zuo, L.; Feng, Y.; Qian, R.; Qi, Y.; Ji, Y.; Xu, Z., Influence of NaOH content on the alkali conversion mechanism in MSWI bottom ash alkali-activated mortars. *Constr. Build. Mater.* **2020,** 248, 118582.

24. Huang, G.; Ji, Y.; Li, J.; Zhang, L.; Liu, X.; Liu, B., Effect of activated silica on polymerization mechanism and strength development of MSWI bottom ash alkali-activated mortars. *Constr. Build. Mater.* **2019,** 201, 90-99.

25. Huang, G.; Ji, Y.; Zhang, L.; Li, J.; Hou, Z., The influence of curing methods on the strength of MSWI bottom ash-based alkali-activated mortars: The role of leaching of OH− and free alkali. *Constr. Build. Mater.* **2018,** 186, 978-985.

26. Alderete, N. M.; Joseph, A. M.; Van den Heede, P.; Matthys, S.; De Belie, N., Effective and sustainable use of municipal solid waste incineration bottom ash in concrete regarding strength and durability. *Resour. Conserv. Recy.* **2021,** 167, 105356.

27. Maldonado-Alameda, A.; Giro-Paloma, J.; Svobodova-Sedlackova, A.; Formosa, J.; Chimenos, J. M., Municipal solid waste incineration bottom ash as alkali-activated cement precursor depending on particle size. *J. Clean. Prod.* **2020,** 242, 118443.

28. Tian, X.; Rao, F.; León-Patiño, C. A.; Song, S., Effects of aluminum on the expansion and microstructure of alkali-activated MSWI fly ash-based pastes. *Chemosphere* **2020,** 240, 124986.

29. Carvalho, R.; Silva, R. V.; de Brito, J.; Pereira, M. F. C., Alkali activation of bottom ash from municipal solid waste incineration: Optimization of NaOH- and Na 2SiO3-based activators. *J. Clean. Prod.* **2021,** 291, 125930.

30. Casanova, S.; Silva, R. V.; de Brito, J.; Pereira, M. F. C., Mortars with alkali-activated municipal solid waste incinerator bottom ash and fine recycled aggregates. *J. Clean. Prod.* **2021,** 289, 125707.

31. Teo, P. T.; Zakaria, S. K.; Salleh, S. Z.; Taib, M. A. A.; Mohd Sharif, N.; Abu Seman, A.; Mohamed, J. J.; Yusoff, M.; Yusoff, A. H.; Mohamad, M., Assessment of electric arc furnace (EAF) steel slag waste's recycling options into value added green products: A review. *Metals* **2020,** 10, (10), 1347.

32. Fisher, L. V.; Barron, A. R., The recycling and reuse of steelmaking slags—A review. *Resour. Conserv. Recy.* **2019,** 146, 244-255.

33. Autelitano, F.; Giuliani, F., Electric arc furnace slags in cement-treated materials for road construction: Mechanical and durability properties. *Constr. Build. Mater.* **2016,** 113, 280-289.

34. Manso, J. M.; Gonzalez, J. J.; Polanco, J. A., Electric arc furnace slag in concrete. *J. Mater. Civ. Eng.* **2004,** 16, (6), 639-645.

35. EN-197-1, Cement - Part 1: Composition, specifications and conformity criteria for common cements. Comité Européen de Normalisation (CEN): Brussels, Belgium, 2011; p 50.

36. EN-1338, Concrete paving blocks - Requirements and test methods. Comité Européen de Normalisation (CEN): Brussels, Belgium, 2003; p 76.

37. Provis, J. L.; van Deventer, J. S. J., *Alkali Activated Materials - State-of-the-Art Report, RILEM TC 224-AAM*. Springer: The Netherlands, 2014; p 388.

38. Bernal, S. A.; Provis, J. L.; Mejía de Gutiérrez, R.; van Deventer, J. S. J., Accelerated carbonation testing of alkali-activated slag/metakaolin blended concretes: effect of exposure conditions. *Mater. Struct.* **2015,** 48, (3), 653-669.

39. Bernal, S. A.; Provis, J. L.; Walkley, B.; San Nicolas, R.; Gehman, J. D.; Brice, D. G.; Kilcullen, A. R.; Duxson, P.; van Deventer, J. S. J., Gel nanostructure in alkali-activated binders based on slag and fly ash, and effects of accelerated carbonation. *Cem. Concr. Res.* **2013,** 53, 127-144.

40. Li, Z.; He, Z.; Shao, Y., Early age carbonation heat and products of tricalcium silicate paste subject to carbon dioxide curing. *Materials* **2018,** 11, (5), 730.

41. Avila, Y.; Silva, R. V.; de Brito, J., Alkali-Activated Materials with Pre-Treated Municipal Solid Waste Incinerator Bottom Ash. **2022,** 12, (7), 3535.

Lisboa, 22nd August, 2022

Authors

Dany Azad Kareem Kassim	Ghandy Lamaa
PhD Student	PhD Student
Rui Vasco Silva	Jorge de Brito
PhD Researcher	Full Professor